

CaMn_{0.5}Ir_{0.5}O_{2.5} – an Ir³⁺ containing anion-deficient perovskite oxide.

Jacob E. Page and Michael A. Hayward *

Department of Chemistry, University of Oxford, Inorganic Chemistry Laboratory, South Parks Road, Oxford, OX1 3QR, U.K.

ABSTRACT: Reaction between CaMn_{0.5}Ir_{0.5}O₃ and NaH, either through solid-solid contact or via a gas mediated reaction process, yields the topochemically reduced phase CaMn_{0.5}Ir_{0.5}O_{2.5} in which Mn³⁺ and Ir³⁺ cations are located within a partially anion-vacancy disordered lattice. Magnetization data from CaMn_{0.5}Ir_{0.5}O_{2.5} can be fit by the Curie-Weiss law to yield $C = 1.586 \text{ cm}^3 \text{ K mol}^{-1}$ and $\theta = -86.9 \text{ K}$, consistent with a combination of $S = 2 \text{ Mn}^{3+}$ and $S = 0 \text{ Ir}^{3+}$. On cooling below $T \sim 110 \text{ K}$ the system undergoes a transition to a spin-glass state, consistent with the observed Mn/Ir cation disorder and frustration between Mn-O-Mn and Mn-O-Ir-O-Mn magnetic couplings. The degree of reduction and the observed anion-vacancy disorder are discussed on the basis of the d-orbital filling of the transition metal cations.

Introduction

Complex transition metal oxides exhibit a wide variety of chemical and physical properties principally due to the presence of unpaired electrons which reside in transition-metal d-orbitals. By controlling the d-electron counts (*via* metal oxidation states) and relative d-orbital energies (*via* crystal field effects arising from coordinated ligands) we can induce these d-electrons to interact strongly with each other to yield collective correlated electronic behavior and properties such as superconductivity, spin-polarized conductivity and magnetoresistance.¹

It therefore follows that a key mechanism by which the physical and chemical behavior of transition metal oxides can be tuned is through the manipulation of metal oxidation states and local coordination environments. However, the high-temperature regimes under which most complex oxides are prepared severely limit the variety of values these parameters can take, restricting them to the most thermodynamically stable combinations and thus curtailing the chemical diversity of complex transition-metal oxides and the physical and chemical properties they can exhibit.

Topochemical reduction *via* anion deintercalation offers opportunities to prepare complex transition-metal oxides with metal cations in unusually low oxidation states and residing in sites with unusual local coordination numbers and geometries, because these processes operate under kinetic rather than thermodynamic product selection conditions and therefore allow the preparation of metastable compounds.² By using this approach highly metastable phases containing novel local configurations such as square-planar Ni¹⁺, Co¹⁺, Fe²⁺, Ru²⁺ or Ir²⁺ can be prepared.³⁻⁸ Building on these observations, and to make the most of this preparative route it is important to have some predictability and control over the anion-deficient phases formed so desired target materials can be prepared.

Recently we have been investigating the topochemical reduction of complex oxides containing 4d and 5d transition-metal cations and have observed that when a phase *only* con-

tains 4d or 5d metals it is extremely challenging to prevent the non-topochemical reduction/decomposition of a phase to the elemental metal. Thus for example SrRuO₃ is reduced to SrO + Ru, not SrRuO_{3-x},⁷ or Sr₂IrO₄ is reduced to SrO + Ir, not Sr₂IrO_{4-x}.⁸ However by including a 3d transition metal along with the 4d/5d metal, topochemically reduced phases can be prepared. For example SrFe_{0.5}Ru_{0.5}O₃ and LaSrNiRuO₆ can be converted to SrFe_{0.5}Ru_{0.5}O₂ and LaSrNiRuO₄ respectively,^{7, 9} while Sr₂FeIrO₆ and Sr₂Co_{0.5}Ir_{0.5}O₄ can be converted to Sr₂FeIrO₄ and Sr₂Co_{0.5}Ir_{0.5}O₃ respectively.^{8, 10}

The inclusion of a 3d transition-metal not only provides a method to help stabilize topochemically reduced phases, but could also provides a mechanism to direct the products of the topochemical reaction towards desired phases. Taking the iridium systems as an example, we observe that both in the Sr₂FeIrO₆ perovskite and A₂M_{0.5}Ir_{0.5}O₄ (M = Fe, Co) Ruddlesden-Popper systems, octahedral Ir⁵⁺ is reduced to square-planar Ir²⁺ with concomitant reduction of the 3d metals to square-planar Fe²⁺/Co²⁺/Co¹⁺.^{8, 10} These transformations must pass through hypothetical Ir³⁺ phases, but these have not been isolated to date. By changing the identity of the 3d metal, could we facilitate the isolation of these Ir³⁺ phases?

Here we describe the topochemical reduction of the perovskite phase CaMn_{0.5}Ir_{0.5}O₃ to CaMn_{0.5}Ir_{0.5}O_{2.5} in which the inclusion of Mn helps to stabilize Ir³⁺ centers in the topochemically reduced phase.

Experimental

Synthesis of CaMn_{0.5}Ir_{0.5}O₃. Samples of CaMn_{0.5}Ir_{0.5}O₃ were prepared using a citrate gel method. Appropriate quantities of CaCO₃ (99.999%) and MnO₂ (99.997%) were dissolved in a minimal quantity of a 1:1 mixture of conc. nitric acid and distilled water, then the required amount of IrO₂ (99.99%, dried at 700 °C for 2 hours) was added. Citric acid and ethylene glycol were then added and the solution was heated whilst being stirred. The gel thus formed was allowed to dry and combust in air. The resulting product was ground into a fine powder, placed in an alumina crucible and heated at a rate

of $1\text{ }^{\circ}\text{C min}^{-1}$ to $1000\text{ }^{\circ}\text{C}$ in air to remove the organic components of the sample. The powder was then pressed into pellets and heated in air at $1100\text{ }^{\circ}\text{C}$ for two periods of 2 days, with grinding between heating periods. The resulting powder was observed to be phase-pure by laboratory X-ray powder diffraction, with lattice parameters $a = 5.3758(1)\text{ }\text{\AA}$, $b = 5.4699(1)\text{ }\text{\AA}$, $c = 7.6408(1)\text{ }\text{\AA}$ in good agreement with values reported in the literature.¹¹

Reduction of $\text{CaMn}_{0.5}\text{Ir}_{0.5}\text{O}_3$. Small samples of $\text{CaMn}_{0.5}\text{Ir}_{0.5}\text{O}_3$ ($\sim 200\text{ mg}$) were mixed with two mole-equivalents of NaH using an agate pestle and mortar in an argon filled glovebox. The mixtures were then placed in Pyrex tubes, sealed under vacuum and heated at temperatures in the range $150 \leq T / ^{\circ}\text{C} \leq 210$ with reaction progress followed using X-ray powder diffraction. Once a reaction was deemed to have reached completion the products were washed with $4 \times 100\text{ ml}$ of clean methanol, under an inert atmosphere, in order to remove sodium-containing by products (NaOH) and any remaining NaH. The samples were then dried under vacuum.

An alternate method was used to reduce large samples ($\sim 1.5\text{ g}$) of $\text{CaMn}_{0.5}\text{Ir}_{0.5}\text{O}_3$ in which the material to be reduced was placed in glass ‘thimble’ which was then sealed in an evacuated Pyrex tube with 1 mole equivalent of NaH, so that the $\text{CaMn}_{0.5}\text{Ir}_{0.5}\text{O}_3$ and NaH shared an atmosphere, but were not in physical contact – i.e. a ‘getter’ set up. The reaction apparatus was then heated for 4 periods of 7 d at $200\text{ }^{\circ}\text{C}$, with the sample being reground and the NaH replaced with fresh material between heating periods.

Characterization. X-ray powder diffraction data were collected from samples contained in gas-tight sample holders using a PANalytical X’Pert diffractometer incorporating an X’celerator position sensitive detector (monochromatic Cu K α 1 radiation). High-resolution synchrotron X-ray powder diffraction data were collected using instrument I11 at the Diamond Light Source Ltd. Diffraction patterns were collected using Si-calibrated X-rays with an approximate wavelength $0.825\text{ }\text{\AA}$, from samples sealed in 0.3 mm diameter borosilicate glass capillaries. Neutron powder diffraction data were collected using the D2b instrument (ILL neutron source, France) from samples contained within vanadium cans sealed under argon. Rietveld profile refinements were performed using the GSAS suite of programs.¹² DC magnetization data were collected using a Quantum Design MPMS SQUID magnetometer. Thermogravimetric measurements were performed by heating powder samples at a rate of $5\text{ }^{\circ}\text{C min}^{-1}$ under a flowing oxygen atmosphere, using a Mettler-Toledo MX1 thermogravimetric microbalance.

Results

Formation and stability of $\text{CaMn}_{0.5}\text{Ir}_{0.5}\text{O}_{3-x}$. Samples of physically mixed $\text{CaMn}_{0.5}\text{Ir}_{0.5}\text{O}_3$ and NaH heated in the temperature range $150 < T/^{\circ}\text{C} < 190$ showed no obvious signs of reaction by X-ray powder diffraction, while samples heated at temperatures above $210\text{ }^{\circ}\text{C}$ underwent non-topochemical reactions resulting in the formation of elemental Fe and Ir. However, when samples were heated at $200\text{ }^{\circ}\text{C}$ an orthorhombic phase ($a = 5.41\text{ }\text{\AA}$, $b = 7.62\text{ }\text{\AA}$, $c = 5.39\text{ }\text{\AA}$) was formed. Unfortunately, when the products of this reaction were washed with methanol to remove NaOH/NaH, large quantities of finely divided Ir metal were formed (in common with behavior observed during the synthesis of $\text{Sr}_2\text{FeIrO}_4$)⁸. Attempts to modify the washing procedure to avoid sample decomposition, by acidifying the solution with NH_4Cl , were unsuccessful. To

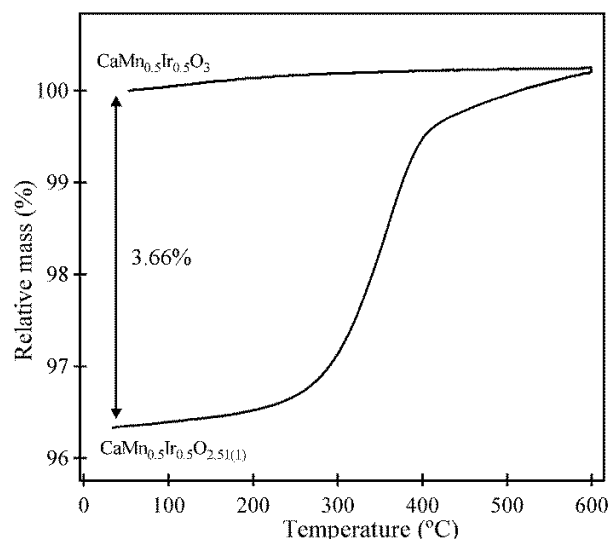


Figure 1. Thermogravimetric data collected during the reoxidation of $\text{CaMn}_{0.5}\text{Ir}_{0.5}\text{O}_{2.5}$ to $\text{CaMn}_{0.5}\text{Ir}_{0.5}\text{O}_3$.

avoid the need for a washing step a getter-type reaction procedure, described above, was adopted and this allowed the preparation of the same orthorhombic phase as prepared by physically mixing the $\text{CaMn}_{0.5}\text{Ir}_{0.5}\text{O}_3$ and NaH, enabling this reduced phase to be isolated.

Structural and Chemical Characterization of $\text{CaMn}_{0.5}\text{Ir}_{0.5}\text{O}_{2.5}$. Thermogravimetric data collected while heating the reduced $\text{CaMn}_{0.5}\text{Ir}_{0.5}\text{O}_{3-x}$ phase under flowing oxygen to reform $\text{CaMn}_{0.5}\text{Ir}_{0.5}\text{O}_{3.00}$ (confirmed by X-ray powder diffraction) indicate the composition of $\text{CaMn}_{0.5}\text{Ir}_{0.5}\text{O}_{2.51(1)}$, as shown in Figure 1. The reduced phase will henceforth be referred to as $\text{CaMn}_{0.5}\text{Ir}_{0.5}\text{O}_{2.5}$.

Synchrotron X-ray and neutron powder diffraction data collected from $\text{CaMn}_{0.5}\text{Ir}_{0.5}\text{O}_{2.5}$ at ambient temperature can be indexed using an orthorhombic unit cell ($a = 5.4160(7)\text{ }\text{\AA}$, $b = 7.6268(7)\text{ }\text{\AA}$, $c = 5.3892(6)\text{ }\text{\AA}$) with extinction conditions consistent with the $Pnma$ space group of the parent $\text{CaMn}_{0.5}\text{Ir}_{0.5}\text{O}_3$ phase. A model based on the structure of $\text{CaMn}_{0.5}\text{Ir}_{0.5}\text{O}_3$ (space group $Pnma$) was constructed and simultaneously refined against the X-ray and neutron powder diffraction data to help mitigate the effects of the modest signal-to-noise ratio of the neutron diffraction data arising from the large neutron absorption cross-section of Ir. All atomic positional and displacement parameters were refined along with the oxygen occupation factors, which were constrained to respect the composition determined by thermogravimetric analysis. Refinement of these later parameters led to a dramatic improvement in the fit to the data and revealed that the oxygen vacancies were located on the $8d\text{ O}(2)$ anion site with the $4c\text{ O}(1)$ site remaining fully occupied within error. The combined refinement converged smoothly to give a good statistical fit ($\chi^2 = 1.588$). Full details of the refined structure are given in Table 1, with selected bond lengths in Table 2 and plots of the observed and calculated data shown in Figure 2.

Magnetic Characterization. Zero-field-cooled (ZFC) and field-cooled (FC) magnetization data were collected from $\text{CaMn}_{0.5}\text{Ir}_{0.5}\text{O}_{2.5}$ as a function of temperature in an applied field of 100 Oe (Figure 3). Data in the temperature range $125 < T/\text{K} < 300$ can be fitted by the Curie-Weiss law ($\chi = C/(T-\theta)$) to yield values of $C = 1.586(6)\text{ cm}^3\text{ K mol}^{-1}$ and $\theta = -86.8(9)\text{ K}$.

Atom	site	x	y	z	Fraction	U_{iso} (\AA^2)
Ca	4c	0.028(1)	$\frac{1}{4}$	0.999(3)	1	0.028(1)
Mn/Ir	4b	0	0	$\frac{1}{2}$	0.5/0.5	0.011(2)
O(1)	4c	0.475(2)	$\frac{1}{4}$	0.052(2)	0.99(2)	0.052(2)
O(2)	8d	0.206(1)	0.544(1)	0.216(1)	0.75(1)	0.063(2)
CaMn _{0.5} Ir _{0.5} O _{2.5} - Space Group: <i>Pnma</i> (#62)						
Formula weight = 203.66 g mol ⁻¹						
$a = 5.4160(7)$ \AA , $b = 7.6268(7)$ \AA , $c = 5.3892(6)$ \AA ,						
volume = 222.61(5) \AA^3						
Radiation source: Neutron, $\lambda = 1.594$ \AA						
Synchrotron X-ray, $\lambda = 0.8268$ \AA						
Temperature: Room temperature						
$\chi^2 = 1.588$; $wRp = 3.98$ %; $Rp = 2.83$ %.						

Table 1. Structural parameters from the combined refinement of CaMn_{0.5}Ir_{0.5}O_{2.5} against synchrotron X-ray and neutron powder diffraction data.

Cation	Anion	length (\AA)
Ca	O(1)	2.438(12)
	O(1)	2.437(19)
	O(1)	2.983(19)
	O(1)	3.009(12)
	O(2)	$2.327(11) \times 2$
	O(2)	$2.621(12) \times 2$
	O(2)	$2.706(10) \times 2$
Mn/Ir	O(1)	$1.932(2) \times 2$
	O(2)	$1.924(5) \times 1.5$
	O(2)	$2.001(5) \times 1.5$
	Bond Angle ($^\circ$)	
Mn/Ir-O(1)-Mn/Ir	161.4(1)	
Mn/Ir-O(2)-Mn/Ir	153.5(3)	

Table 2. Selected bond lengths and angles from the refined structure of CaMn_{0.5}Ir_{0.5}O_{2.5}.

The value of the Curie constant is close to that expected from a combination of $S = 2$ Mn³⁺ and $S = 0$ Ir³⁺ ($C_{\text{calc}} = 1.5 \text{ cm}^3 \text{ K mol}^{-1}$). Below $T = 110$ K the ZFC and FC data diverge strongly, indicative of a change in magnetic behavior. A magnetization-field isotherm (± 5 T) collected at 300 K is linear and passes through the origin, consistent with CaMn_{0.5}Ir_{0.5}O_{2.5} being a simple paramagnet at this temperature (Figure 4). In contrast, analogous data collected at 5 K, after cooling in an applied field of 5 T, exhibit hysteresis and are displaced from the origin indicating spin-glass behavior for CaMn_{0.5}Ir_{0.5}O_{2.5}. Neutron diffraction data collected at 5 K show no additional diffraction features compared to the data collected at 300 K.

Discussion

Mechanism of CaMn_{0.5}Ir_{0.5}O₃ reduction. Reaction between CaMn_{0.5}Ir_{0.5}O₃ and NaH yields the topochemically reduced phase CaMn_{0.5}Ir_{0.5}O_{2.5} if the two powders are in direct physical contact (solid-solid reaction) or if they just share a common atmosphere (getter reaction). The reactivity when the

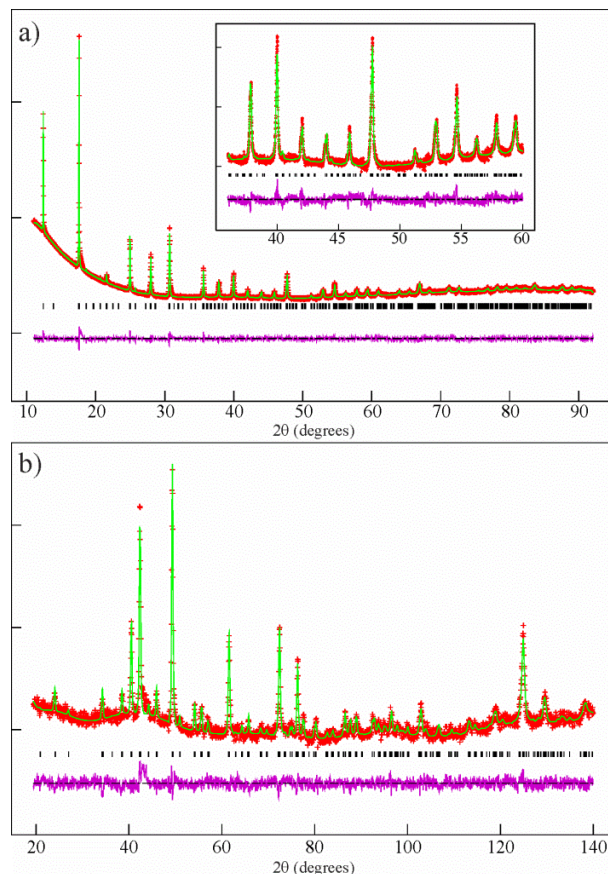


Figure 2. Observed calculated and difference plots from the combined structural refinement of CaMn_{0.5}Ir_{0.5}O_{2.5} against a) synchrotron X-ray and b) neutron powder diffraction data.

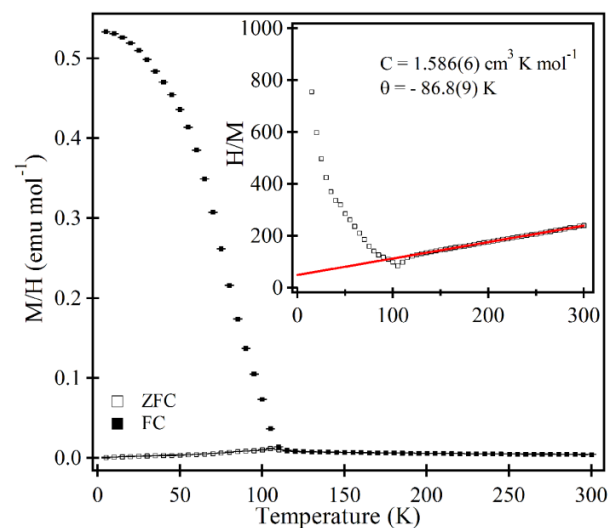


Figure 3. Zero-field cooled and field cooled magnetization data collected from CaMn_{0.5}Ir_{0.5}O_{2.5} in an applied field of 100 Oe. Inset shows fit to the Curie-Weiss law.

reagents are physically separated clearly shows that there can be a gas-phase component to the reaction. In principal, there are two basic mechanisms that could be operating which include a gas-phase component: i) On heating CaMn_{0.5}Ir_{0.5}O₃ releases oxygen gas which then reacts with the NaH to form

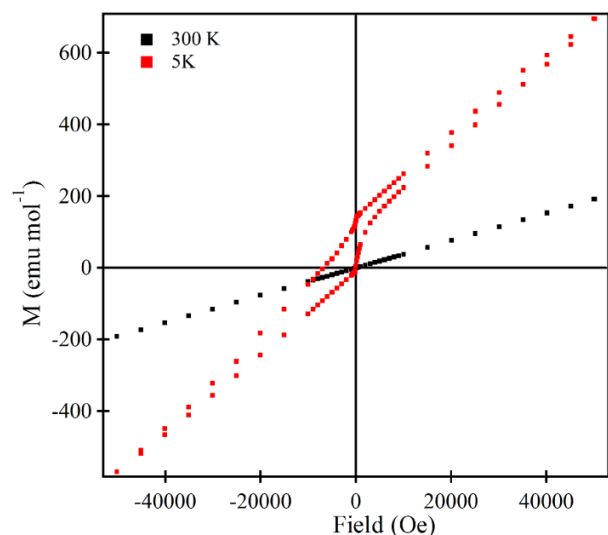


Figure 4. Magnetization field data collected from $\text{CaMn}_{0.5}\text{Ir}_{0.5}\text{O}_{2.5}$. Data were collected at 5 K after cooling from 300 K in an applied field of 50,000 Oe.

NaOH, or ii) NaH releases hydrogen which reacts with $\text{CaMn}_{0.5}\text{Ir}_{0.5}\text{O}_3$ to form water which then transfers back to the Na/NaH to further react to form NaOH.

Similar ‘gas mediated’ reactivity has been observed during the reduction of SrFeO_3 to SrFeO_2 using physically separated CaH_2 ,¹³ and it was concluded that the most likely mechanism in this case proceeded *via* the release of H_2 by CaH_2 analogous to mechanism ii) above. This also appears to be the most likely mechanism for the $\text{CaMn}_{0.5}\text{Ir}_{0.5}\text{O}_3$ -NaH reaction given that it is possible to reduce the iridium complex-oxide $\text{Sr}_2\text{FeIrO}_6$ to $\text{Sr}_2\text{FeIrO}_4$ with dilute hydrogen gas.⁸ It should be noted that in both the SrFeO_3 - CaH_2 and $\text{CaMn}_{0.5}\text{Ir}_{0.5}\text{O}_3$ -NaH systems the reduction reaction is observed to proceed much more rapidly when the reagents are in physical contact (i.e. when a solid-solid reaction is possible) suggesting that under these conditions a faster all-solid-state mechanism is in operation. However the observation that ‘getter type’ reactions using metal hydrides can yield topochemically reduced phases gives synthetic chemists additional options, which are especially useful in cases like the reduction of $\text{CaMn}_{0.5}\text{Ir}_{0.5}\text{O}_3$ to $\text{CaMn}_{0.5}\text{Ir}_{0.5}\text{O}_{2.5}$ where the post-synthesis separation of reagents leads to sample decomposition.

Reduction level. The conversion of $\text{CaMn}_{0.5}\text{Ir}_{0.5}\text{O}_3$ to $\text{CaMn}_{0.5}\text{Ir}_{0.5}\text{O}_{2.5}$ appears to be the maximum level of topochemical reduction achievable either in solid-solid or getter type reaction modes, as raising the reaction temperature leads to non-topochemical reactions and the formation of elemental Fe and Ir in either reaction set up. It is surprising that the level of reduction is limited to a $\text{Mn}^{3+}/\text{Ir}^{3+}$ oxidation state combination as hydride reducing agents have been shown to be capable of preparing Ir^{2+} , Mn^{2+} and even Mn^{1+} containing phases via the topochemical reduction of complex oxides.^{8, 14–17} The lack of further reduction in the $\text{CaMn}_{0.5}\text{Ir}_{0.5}\text{O}_{3-x}$ system can be rationalized by observing that if the anion vacancy concentration rises above 16% ($x > 0.5$) the average coordination number of the transition metal cations must fall below 5. Typically, 4-coordinate transition metal centers reside in square-planar coordination sites in topochemically reduced perovskite phases, as exemplified by the Ni^{1+} and Fe^{2+} cations within the infinite layer structures of LaNiO_2 and SrFeO_2 .^{3, 5} However, to

date there are no examples of manganese cations adopting square-planar coordinations in topochemically reduced oxides (although there are examples of square-planar manganese centers in mixed anion and non-topochemically prepared systems).[ref] Indeed the partial substitution of manganese for iron in $\text{SrFe}_{1-x}\text{Mn}_x\text{O}_{3-y}$ prevents its conversion to $\text{SrFe}_{1-x}\text{Mn}_x\text{O}_2$ for values of $x > 0.3$,¹⁸ confirming the formation of square-planar Mn^{2+} is disfavored. In contrast square-planar Ir^{2+} has been observed in $\text{Sr}_2\text{FeIrO}_4$ and $\text{A}_2\text{M}_{0.5}\text{Ir}_{0.5}\text{O}_3$ phases,^{8, 10} thus we can attribute the lack of further reduction beyond $\text{CaMn}_{0.5}\text{Ir}_{0.5}\text{O}_{2.5}$ to the unfavorability of forming square-planar Mn^{2+} centers, which limits the composition at this value, stabilizing the formation of Ir^{3+} .

Anion-vacancy disorder. Neutron powder diffraction data indicate that the oxide ion vacancies present in $\text{CaMn}_{0.5}\text{Ir}_{0.5}\text{O}_{2.5}$ are located within a single plane of the host perovskite lattice. Thus on reduction the stacking sequence changes from $-\text{CaO}-(\text{Mn}_{0.5}\text{Ir}_{0.5})\text{O}_2-\text{CaO}-(\text{Mn}_{0.5}\text{Ir}_{0.5})\text{O}_2-$ in $\text{CaMn}_{0.5}\text{Ir}_{0.5}\text{O}_3$ to $-\text{CaO}-(\text{Mn}_{0.5}\text{Ir}_{0.5})\text{O}_{1.5}-\text{CaO}-(\text{Mn}_{0.5}\text{Ir}_{0.5})\text{O}_{1.5}-$ in $\text{CaMn}_{0.5}\text{Ir}_{0.5}\text{O}_{2.5}$ as shown in Figure 5a. This localization of anion vacancies is reminiscent of the analogous all-manganese phase $\text{CaMnO}_{2.5}$ (prepared via the topochemical reduction of CaMnO_3) which adopts an analogous $-\text{CaO}-\text{MnO}_{1.5}-\text{CaO}-\text{MnO}_{1.5}-$ structural stacking sequence,^{19–20} although the anion vacancies are ordered within the $\text{MnO}_{1.5}$ planes of $\text{CaMnO}_{2.5}$ but disordered within the $(\text{Mn}_{0.5}\text{Ir}_{0.5})\text{O}_{1.5}$ sheets of $\text{CaMn}_{0.5}\text{Ir}_{0.5}\text{O}_{2.5}$, as shown in Figures 5b and 5c.

We can understand the change from anion-vacancy order to disorder on iridium-for-manganese substitution in the $\text{Ca}(\text{Mn}/\text{Ir})\text{O}_{2.5}$ system by examining the structures of the phases closely. The rigorous anion-vacancy order present in $\text{CaMnO}_{2.5}$ can be attributed to the need to minimize the lattice strain arising from the large difference between the lengths of the apical Mn-O bonds (2.091 Å), which lie *trans* to the anion vacancy site, and the 4 equatorial Mn-O bonds (2×1.926 Å, 2×1.883 Å) which are *cis* to the anion vacancy sites of this phase.^{19–20} By aligning the pairs of long apical Mn-O bonds, which lie *trans* to each anion vacancy in a ‘herring bone’ pattern in the xy plane, as indicated by the red and blue arrows in Figure 5c, lattice strain is minimized. The large elongation of the apical Mn-O bonds arises in part from a Jahn-Teller like distortion of the d^4 Mn^{3+} centers, so it can be seen that the anion-vacancy order is coupling to, and stabilized by, the Mn^{3+} orbital order (ordered Jahn-Teller distortion) present in $\text{CaMnO}_{2.5}$.

The $(\text{Mn}/\text{Ir})\text{O}_{6-x}$ polyhedra in the anion-vacancy disordered structure of $\text{CaMn}_{0.5}\text{Ir}_{0.5}\text{O}_{2.5}$ also exhibit an ordered distortion to give 2 extended apical (Mn/Ir)-O bonds (2.001(5) Å) and 4 contracted equatorial (Mn/Ir)-O bonds ($2 \times 1.932(2)$ Å, $2 \times 1.924(5)$ Å) as detailed in Table 2. However the bond length distortion in $\text{CaMn}_{0.5}\text{Ir}_{0.5}\text{O}_{2.5}$ is considerably smaller (axial/equatorial = 1.037) than that observed for $\text{CaMnO}_{2.5}$ (axial/equatorial = 1.097) and furthermore, the arrangement of long axial and short equatorial bonds within the $\text{Mn}_{0.5}\text{Ir}_{0.5}\text{O}_{2.5}$ planes of $\text{CaMn}_{0.5}\text{Ir}_{0.5}\text{O}_{2.5}$ changes to the CE-type order observed for LaMnO_3 ,²¹ indicated by the red and blue arrows in Figure 5b. In this arrangement all the extended axial bonds on neighboring Mn/Ir centers are perpendicular, and as a result all the anion sites within the $\text{Mn}_{0.5}\text{Ir}_{0.5}\text{O}_{1.5}$ planes are symmetry equivalent so the orbital order cannot direct and stabilize any anion-vacancy order. Thus we can attribute the lack of rigorous anion vacancy order in $\text{CaMn}_{0.5}\text{Ir}_{0.5}\text{O}_{2.5}$ to the disruption of

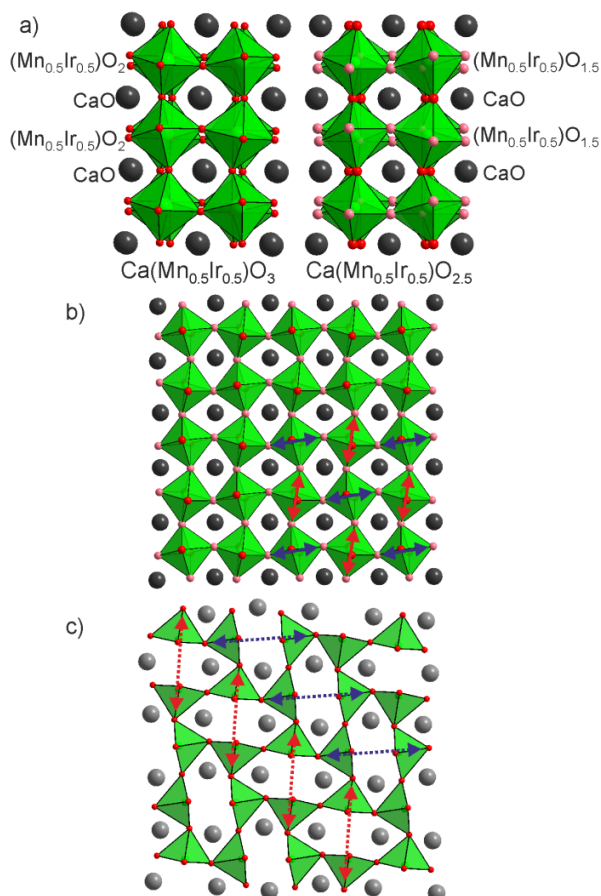


Figure 5 The structures of a) $\text{CaMn}_{0.5}\text{Ir}_{0.5}\text{O}_3$ and $\text{CaMn}_{0.5}\text{Ir}_{0.5}\text{O}_{2.5}$ illustrating the location of the anion-vacancies in the latter structure. Black, green, red and pink spheres represent Ca^{2+} , $\text{Mn}^{3+}/\text{Ir}^{3+}$, fully occupied and partially occupied oxide anion sites respectively; b) the anion-vacancy disordered $\text{Mn}_{0.5}\text{Ir}_{0.5}\text{O}_{1.5}$ layers of $\text{CaMn}_{0.5}\text{Ir}_{0.5}\text{O}_{2.5}$ and c) the anion-vacancy ordered $\text{MnO}_{1.5}$ layers of $\text{CaMnO}_{2.5}$. Red and blue arrows indicate the orientation and ordering of the long apical (Mn/Ir)-O bonds within these layers.

the Mn^{3+} orbital order by substitution of Jahn-Teller inactive Ir^{3+} centers, which weaken the average elongation of the (Mn/Ir)-O bond *trans* to anion vacancy sites, weakening the coupling between the orbital order and anion-vacancy order, and ultimately resulting in anion-vacancy disordered structure for $\text{CaMn}_{0.5}\text{Ir}_{0.5}\text{O}_{2.5}$.

Close inspection of the neutron diffraction data collected from $\text{CaMn}_{0.5}\text{Ir}_{0.5}\text{O}_{2.5}$ (Figure 2) reveals broad additional features in the background of this data set, suggesting the could be some short range order in the phase, not described by the refined ‘average’ structure. The absence of these features in the synchrotron X-ray data further suggests if there are short-range ordered features, they are most likely associated with the anion lattice. These observations in combination suggest there could be some short range ordering of the anion vacancies present in $\text{CaMn}_{0.5}\text{Ir}_{0.5}\text{O}_{2.5}$, unfortunately the curtailed Q-range of the neutron diffraction data set prevents a detailed real-space analysis to investigate this.

Magnetic behavior. The spin-glass behavior observed for $\text{CaMn}_{0.5}\text{Ir}_{0.5}\text{O}_{2.5}$ can also be attributed to the disruption of the Mn^{3+} orbital order by Ir^{3+} substitution. As noted above the

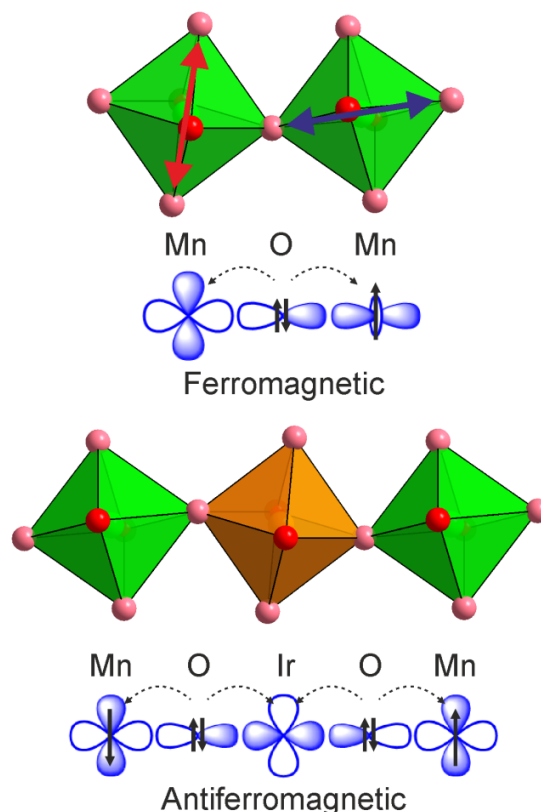


Figure 6. Magnetic exchange interactions present in $\text{CaMn}_{0.5}\text{Ir}_{0.5}\text{O}_{2.5}$.

arrangement of long and short (Mn/Ir)-O bonds within the $\text{Mn}_{0.5}\text{Ir}_{0.5}\text{O}_{1.5}$ planes of $\text{CaMn}_{0.5}\text{Ir}_{0.5}\text{O}_{2.5}$ is consistent with CE-type orbital order of the Mn^{3+} cations. In this configuration the Goodenough-Kanamori rules²² predict all the in-plane Mn-O-Mn and Mn-□-Mn exchange couplings (where □ indicates an anion vacancy) should be ferromagnetic as the half-filled d_{z^2} orbitals are aligned to interact with the empty $d_{x^2-y^2}$ orbitals. Substitution of Mn^{3+} with low-spin, $S = 0$, Ir^{3+} adds an additional antiferromagnetic Mn-O-Ir-O-Mn coupling, analogous to the Fe-O-Ir-O-Fe coupling observed in $\text{Sr}_2\text{FeIrO}_6$,²³⁻²⁴ as shown in Figure 6. This antiferromagnetic coupling will compete with and frustrate the ferromagnetic Mn-Mn couplings leading to the observed spin-glass behavior.

Conclusions

Topochemical reduction of $\text{CaMn}_{0.5}\text{Ir}_{0.5}\text{O}_3$ yields the $\text{Mn}^{3+}/\text{Ir}^{3+}$ phase $\text{CaMn}_{0.5}\text{Ir}_{0.5}\text{O}_{2.5}$. This contrasts with the transformation of $\text{Sr}_2\text{FeIrO}_6$ to the $\text{Fe}^{2+}/\text{Ir}^{2+}$ phase $\text{Sr}_2\text{FeIrO}_4$ indicating that the presence of manganese rather than iron restricts the level of reduction observed and helps to stabilize the Ir^{3+} centers. This suggests that by judicious selection of 3d metals we can control the oxidation states adopted by 4d and 5d transition metals in topochemically reduced oxides.

AUTHOR INFORMATION

Corresponding Author

* michael.hayward@chem.ox.ac.uk

Author Contributions

The manuscript was written through contributions of all authors
The authors declare no competing financial interests.

ACKNOWLEDGMENT

We thank E. Suard for assistance collecting the neutron powder diffraction data. We thank The Leverhulme Trust grant award RPG-2014-366 “Topochemical reduction of 4d and 5d transition metal oxides” for supporting this work. Experiments at the Diamond Light Source were performed as part of the Block Allocation Group award “Oxford Solid State Chemistry BAG to probe composition-structure-property relationships in solids” (EE13284).

REFERENCES

1. Goodenough, J. B.; Zhou, J.-S., Localized to itinerant transition in transition metal oxides. *Chem. Mater.* **1998**, *10*, 2980-2993.
2. Hayward, M. A., Soft chemistry synthesis of oxides. In *Comprehensive Inorganic Chemistry II*, Reedijk, J.; Poeppelmeier, K. R., Eds. Elsevier: Oxford, 2013; Vol. 2, pp 417-453.
3. Hayward, M. A.; Green, M. A.; Rosseinsky, M. J.; Sloan, J., Sodium hydride as a powerful reducing agent for topotactic oxide deintercalation: synthesis and characterisation of the nickel (I) oxide LaNiO_2 . *J. Am. Chem. Soc.* **1999**, *121*, 8843-8854.
4. Seddon, J.; Suard, E.; Hayward, M., Topotactic reduction of YBaCo_2O_5 and $\text{LaBaCo}_2\text{O}_5$: square-planar Co(I) in an extended oxide. *J. Am. Chem. Soc.* **2010**, *132* (8), 2802-2810.
5. Tsujimoto, Y.; Tassel, C.; Hayashi, N.; Watanabe, T.; Kageyama, H.; Yoshimura, K.; Takano, M.; Ceretti, M.; Ritter, C.; Paulus, W., Infinite-layer iron oxide with a square-planar coordination. *Nature* **2007**, *450*, 1062-1065.
6. Dixon, E.; Hayward, M., The Topotactic Reduction of $\text{Sr}_3\text{Fe}_2\text{O}_5\text{Cl}_2$ -Square Planar Fe(II) in an Extended Oxide. *Inorg. Chem.* **2010**, *49* (20), 9649-9654.
7. Denis Romero, F.; Burr, S. J.; McGrady, J. E.; Gianolio, D.; Cibir, G.; Hayward, M. A., $\text{SrFe}_{0.5}\text{Ru}_{0.5}\text{O}_2$: square-planar Ru^{2+} in an extended oxide. *J. Am. Chem. Soc.* **2013**, *135*, 1838-1844.
8. Page, J. E.; Morgan, H. W. T.; Zeng, D.; Manuel, P.; McGrady, J. E.; Hayward, M. A., $\text{Sr}_2\text{FeIrO}_4$: square-planar Ir(II) in an extended oxide. *Inorg. Chem.* **2018**, *57*, 13577-13585.
9. Amano Patino, M.; Zeng, D.; Bower, R.; McGrady, J. E.; Hayward, M. A., Coupled electronic and magnetic phase transition in the infinite-layer phase LaSrNiRuO_4 . *Inorg. Chem.* **2016**, *55* (17), 9012-9016.
10. Page, J. E.; Hayward, M. A., Structure and magnetism of $\text{A}_2\text{M}_{0.5}\text{IrV}_{0.5}\text{O}_4$ and topochemically reduced $\text{A}_2\text{M}_{0.5}\text{IrIr}_{0.5}\text{O}_3$ (M = Fe, Co) complex oxides.
11. Mizusaki, S.; Sato, J.; Taniguchi, T.; Nagata, Y.; Lai, S. H.; Lan, M. D.; Ozawa, T. C.; Noro, Y.; Samata, H., Ferromagnetism in $\text{CaMn}_{1-x}\text{Ir}_x\text{O}_3$. *J. Phys.: Condens. Matter* **2008**, *20* (23).
12. Larson, A. C.; Von Dreele, R. B. *General Structure Analysis System*, Los Alamos National Laboratory Report LAUR 86-748: 2000.
13. Kobayashi, Y.; Li, Z. F.; Hirai, K.; Tassel, C.; Loyer, F.; Ichikawa, N.; Abe, N.; Yamamoto, T.; Shimakawa, Y.; Yoshimura, K.; Takano, M.; Hernandez, O. J.; Kageyama, H., Gas phase contributions to topochemical hydride reduction reactions. *J. Solid State Chem.* **2013**, *207*, 190-193.
14. Parsons, T. G.; D'Hondt, H.; Hadermann, J.; Hayward, M. A., The synthesis and structural characterisation of $\text{La}_{1-x}\text{A}_x\text{MnO}_{2.5}$ (A = Ba, Sr, Ca) phases – mapping the variants of the brownmillerite structure. *Chem. Mater.* **2009**, *21*, 5527.
15. Hadermann, J.; Abakumov, A.; Adkin, J.; Hayward, M., Topotactic Reduction As a Route to New Close-Packed Anion Deficient Perovskites: Structure and Magnetism of 4H-BaMnO_{2+x} . *J. Am. Chem. Soc.* **2009**, *131* (30), 10598-10604.
16. O'Malley, M.; Lockett, M. A.; Hayward, M. A., Anion vacancy ordering in $\text{Sr}_7\text{Mn}_4\text{O}_{15-x}$ phases. *J. Solid State Chem.* **2007**, *180*, 2851-2858.
17. Dixon, E.; Hadermann, J.; Ramos, S.; Goodwin, A. L.; Hayward, M. A., Mn(I) in an extended oxide - the synthesis and characterisation of $\text{La}_{1-x}\text{A}_x\text{MnO}_2$. *J. Am. Chem. Soc.* **2011**, *133*, 18397-18405.
18. Seiberg, L.; Yamamoto, T.; Tassel, C.; Kobayashi, Y.; Hayashi, N.; Kitada, A.; Sumida, Y.; Watanabe, T.; Nishi, M.; Ohoyama, K.; Yoshimura, K.; Takano, M.; Paulus, W.; Kageyama, H., Fe-site substitution effect on the structural and magnetic properties of SrFeO_2 . *Inorg. Chem.* **2011**, *50*, 3988-3995.
19. Poeppelmeier, K. R.; Leonowicz, M. E.; Longo, J. M., $\text{CaMnO}_{2.5}$ and $\text{Ca}_2\text{MnO}_{3.5}$ - New Oxygen-Defect Perovskite-Type Oxides. *J. Solid State Chem.* **1982**, *44* (1), 89-98.
20. Poeppelmeier, K. R.; Leonowicz, M. E.; Scanlon, J. C.; Longo, J. M.; Yelon, W. B., Structure determination of CaMnO_3 and $\text{CaMnO}_{2.5}$. *J. Solid State Chem.* **1982**, *45*, 71-79.
21. Rodriguez-Carvajal, J.; Hennion, M.; Moussa, F.; Moudén, A. H.; Pinsard, L.; Revcolevschi, A., Neutron-diffraction study of the Jahn-Teller transition in stoichiometric LaMnO_3 . *Phys. Rev. B* **1998**, *57* (6), R3189-R3192.
22. Goodenough, J. B., *Magnetism and the chemical bond*. Wiley: New York, 1963.
23. Battle, P. D.; Blake, G. R.; Gibb, T. C.; Vente, J. F., Structural chemistry and electronic properties of $\text{Sr}_2\text{FeIrO}_6$. *J. Solid State Chem.* **1999**, *145* (2), 541-548.
24. Page, J. E.; Topping, C. V.; Scrimshire, A.; Bingham, P. A.; Blundell, S. J.; Hayward, M. A., Doped $\text{Sr}_2\text{FeIrO}_6$ – phase separation and a $J_{\text{eff}} \neq 0$ state for Ir^{3+} . *Inorg. Chem.* **2018**, *57*, 10303-10311.